Composites Science and Technology 70 (2010) 1628–1636

Contents lists available at ScienceDirect

Composites Science and Technology

journal homepage: www.elsevier.com/locate/compscitech

Dynamic capillary impact on longitudinal micro-flow in vacuum assisted impregnation and the unsaturated permeability of inner fiber tows

Min Li [a,*], Shaokai Wang [a], Yizhuo Gu [a], Zuoguang Zhang [a], Yanxia Li [a], Kevin Potter [b]

[a] Key Laboratory of Aerospace Materials and Performance (Ministry of Education), School of Materials Science and Engineering, Beihang University, Beijing 100191, China
[b] Advanced Composites Centre for Innovation and Science, University of Bristol, University Walk, Bristol BS8 1TR, UK

ARTICLE INFO

Article history:
Received 23 November 2009
Received in revised form 26 May 2010
Accepted 4 June 2010
Available online 9 June 2010

Keywords:
A. Polymer-matrix composites (PMCs)
E. Resin transfer moulding (RTM)
D. Permeability
B. Porosity/Voids

ABSTRACT

This paper addresses issues of the synergetic dynamic effect of capillary force on the longitudinal impregnation driven by external pressures, especially under vacuum assistance. An apparatus was designed to detect the axial infiltration along unidirectional fiber bundles which were all aligned closely to give a representation of micro-flow channel of inner fiber tows. The external driving pressures were controlled sufficiently low, 20–60 kPa, on the order of capillary pressures. Based on the analysis of infiltration velocities under different external pressures, dynamic capillary pressures can be determined experimentally. The results showed that capillary pressures, the most important force of microscopic flow through inner fiber yarns, acted as a drag force on the infiltration flow for vacuum assisted penetration into unidirectional fiber bundles. This unique drag effect is very different from traditional unsaturated infiltration, different from the compressed air driving permeation and the theoretical calculated data in this paper. Moreover, values and even signs of the dynamic capillary pressures varied with the fiber fraction of the assemblies as well as the fluid types. Further analysis demonstrated that the function of capillary pressure was closely related to the capillary number (*Ca*), acting as drag force when *Ca* larger than a critical value, and as a promotive force with smaller *Ca*. Consequently, unsaturated permeabilities of the unidirectional fiber bundles were estimated by taking consideration of both dynamic and quasi-static capillary pressures.

1. Introduction

As one of the cost-effective liquid composite moulding (LCM) processes, vacuum assisted resin transfer moulding (VARTM) process has been recognized as a viable option to manufacture large composite structures with complicated shapes [1]. In the process, a polymeric resin is introduced into the mould cavity by evacuating the mould cavity ahead of the infiltration front, so that resin saturates the dry fibrous reinforcement. Hence, complete filling of the reinforcement, both inter- and inner-fiber tows wetting becomes a major issue, which controls both the quality of the product and the processing time.

In the LCM process, resin impregnation is highly dependent on the permeability of fibrous reinforcement. As an important material parameter, permeability represents the degree of difficulty for a fluid to penetrate a porous medium, determined by the geometry of the fibrous preform, which can be predicted according to empirical equations, such as Carman–Kozeny equation [2], Gebart model [3] and Westhuizen model [4]. However, discrepancies are always observed between data from models and typical experiments [5], which are believed to be caused by neglecting the effect of microscopic flow on the interpretation of the macroscopic impregnation.

It has been known that complicated preform structure induces a dual-scale flow behavior: microscopic flow and macroscopic flow [6–10]. A direct result from this flow competition is entrapment of voids within the fabric [11], especially micro voids formed due to the microscopic capillary effects and low permeability of the fiber tows [12]. Because of the importance of capillary flow in LCM process, a number of studies have paid close attention to the evaluation of capillary pressures. Ahn and Seferis [13] designed an apparatus to measure capillary pressure and transverse permeability of carbon fiber woven fabric preform at low applied pressure. Manson and coworkers [14] reported dynamic variation of the capillary pressure in liquid composite moulding. Amico and Lekakou [15] reported the influence of capillary pressure on estimation of permeability of a plain-weave glass fiber fabric. And recently, Advani and coworkers [16] modeled the capillary action on fiber tow saturation during resin infusion by introducing theoretically-estimated capillary pressure in flow simulation. However, as for the dynamic of penetration flow, capillary pressures are always deemed to act as promotive force, which is found not to be true the cases of vacuum driving impregnation in unidirectional fiber bundles in this study.

* Corresponding author. Tel./fax: +86 10 82339800.
E-mail address: leemy@buaa.edu.cn (M. Li).

0266-3538/$ - see front matter © 2010 Elsevier Ltd. All rights reserved.
doi:10.1016/j.compscitech.2010.06.004

Usually it is acknowledged that capillary number plays a critical role on the dynamic variation of capillary pressure and contact angle. Hoffman [17] reported a dependence of the contact angle on the velocity of the flow front. Weitz et al. [18] found similar behavior when a wetting fluid (water) displaced a nonwetting fluid (decane) in a porous media, measured the capillary pressure drop across the interface between two fluids and its dependence on the velocity. Additionally, Calvo et al. [19] investigated the variation of dynamic capillary pressure in diphasic flows through glass capillaries. From the above, one can see that there are no complete adequate reports on dynamic effect of capillary pressure on penetration flow in fibrous perform, especially the interface shape of the flow front.

This paper aims to explore the behavior of capillary forces impacting on vacuum driven unsaturated micro-flow in unidirectional fiber bundles. Dynamic capillary pressures were evaluated experimentally from penetrations under vacuum as well as compressed air pressure. The meniscus shapes of flow front corresponding to the dynamic capillary pressure were verified by experiments. Relationship between dynamic capillary pressures and the capillary numbers were analyzed by transient velocity measurement. Consequently, the influence of capillary pressure on the accuracy of unsaturated permeability of inner fiber tows was determined.

2. Experimental

2.1. Materials

Axial infiltration experiments were carried out using SC8-12 × 20 glass fiber bundles, supplied by Nanjing Fiberglass Research and Design Institute. Each bundle contains 880 fiber filaments with diameter of 11.9 μm.

The impregnating fluid used in this study was silicone oil from Beijing Chemical Reagents Company. In order to verify the unique drag effect of capillary pressure obtained by silicone oil, different fluids were employed, i.e. soybean oil, epoxy resin and glycerol to repeat the impregnation experiments driven by external vacuum. Table 1 lists properties of all the liquids at ambient temperature, where the viscosity and the surface tension were tested by a Gemini rheometer of Bohlin Instrument and DCAT21 made by Dataphysics Instrument, respectively.

2.2. Equipment and penetration test procedure

Two kinds of apparatus were designed to simulate infiltration flow during LCM process, either driven by vacuum pressure or compressed air pressure, as depicted schematically in Fig. 1. The employed driving pressure was sufficiently low, less than 60 kPa, so that capillary pressure effects could not be neglected. The unidirectional fiber assembly was prepared by loading fibers in the longitudinal direction into a PTFE tube, i.e. preform holder. The inner diameter of the preform holder was 3.8 mm. After the end of the fiber bundle was cut off, the assembly was then pulled into the PTFE preform holder, and the flat end of the fiber assembly was kept 1–2 cm away from the holder end.

Table 1
Properties of infiltration fluids at ambient temperatures.

Liquids	Density (g/cm^3)	Viscosity (Pa s)	Surface tension ($\times 10^{-3}$ N/m)
Silicone oil	0.98	0.24	21.25
Soybean oil	0.92	0.08	33.86
Epoxy resin	1.15	0.65	45.49
Glycerol	1.26	0.53	63.73

The fiber volume fraction V_f is determined by:

$$V_f = \frac{nNS_f}{S_t} \tag{1}$$

where S_f and S_t are cross-sectional areas of the fiber filament and the PTFE tube respectively, n is the number of fiber bundles in the specimen, and N is the number of filaments in one fiber bundle, i.e. 880 in this study. From Eq. (1), tow number n required for a certain fiber volume fraction can be calculated.

For the vacuum driving apparatus, infiltration flow was measured with the preform holder suspended above a liquid reservoir, as shown in Fig. 1a. The preform holder end was dipped into the fluid by rising the elevator platform, and meanwhile the fiber assembly was kept from contacting the liquid. After closing the regulator valve, the vacuum pump started to remove air in both the buffer tank and the pipe until stable vacuum pressure was obtained. Vacuum pressure in the preform holder can reach the same as that in the buffer tank in 2 s after the regulator valve was opened. Once the liquid was introduced into the preform, the rise of fluid height was recorded as a function of time. For the compressed air driving apparatus, the preform holder was connected with a liquid reservoir through a pipe, as illustrated in Fig. 1b. The pressure generated from the air compressor forced the liquid to infiltrate the preform. The rise height readings were recorded with impregnating time.

The infiltration experiments were conducted under different constant pressures. The height of the flow front as a function of time is shown in Fig. 2. As expected, the silicone oil permeates into the glass fiber assembly more quickly under higher external applied pressure. Moreover, it is of interest to note that the infiltration experiments driven by vacuum pressure show larger velocities, in comparison with those driven by compressed air under the same conditions, including fiber volume fractions and the applied pressure.

2.3. Data analysis based on penetration velocities

For the infiltration experiments, the liquid flow is forced by a pressure difference ΔP, which is generated from combined actions of applied pressure, capillary pressure and gravity.

$$\Delta P = P_{\text{app}} + P_c - \rho g h \tag{2}$$

where P_{app} is applied pressure, ρ is the liquid density, g is the gravitational acceleration, h is the height of liquid rise, and P_c is the capillary pressure which arises from the interface tension between liquid and air, as well as the porosity of the fiber assembly.

Assuming that the preform is incompressible and the liquid behaves as a Newtonian fluid, then Darcy's law [20–22] in one-directional form can be used to describe the flow along unidirectional fiber bundles,

$$\frac{dh}{dt} = \frac{K}{\eta(1 - V_f)} \frac{dP}{dh} \tag{3}$$

where K is permeability of the unidirectional fiber bundles, V_f is fiber volume fraction, and η is liquid viscosity. In this study, the fluid was driven by vacuum or compressed air of the values range from 20 kPa to 60 kPa, and length of the unidirectional fiber bundle was no more than 9 cm, which could be totally penetrated in 1 h. Therefore, the hydraulic pressure produced by the absorbed silicone oil turned out to be lower than 900 Pa, far less than the external pressure. Hence, the liquid force of gravity can be negligible. For constant applied pressure, Eq. (3) can be rearranged as:

$$\frac{dh}{dt} = \frac{K}{\eta(1 - V_f)} \frac{(P_{\text{app}} + P_c)}{h}, \tag{4}$$

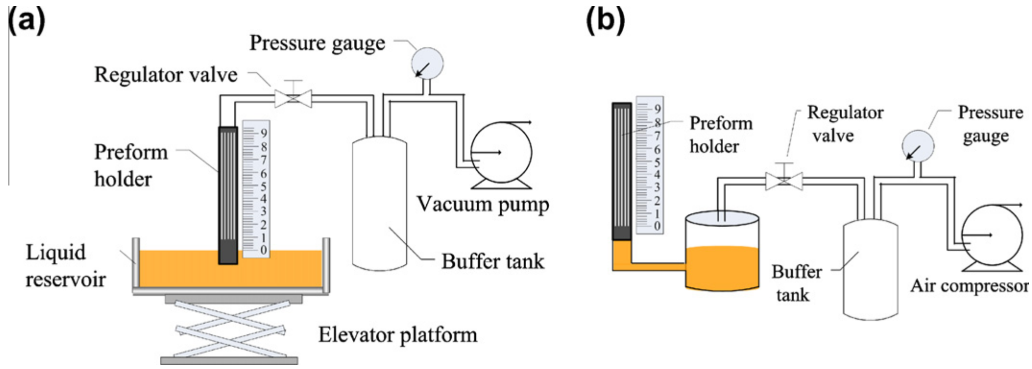

Fig. 1. Schematics of experimental apparatus for infiltration experiments under the assistance of: (a) vacuum and (b) compressed air pressure.

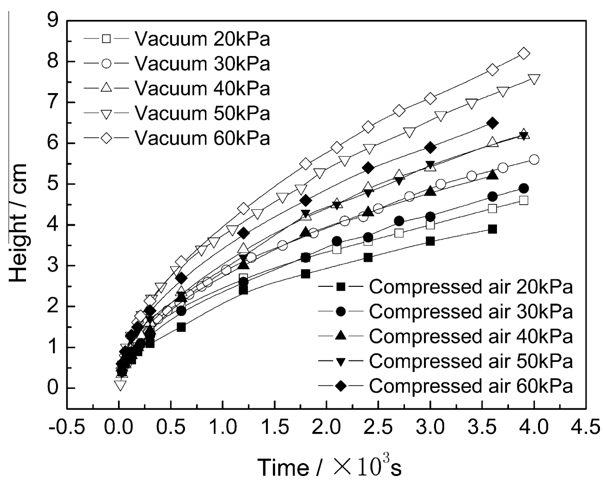

Fig. 2. Height–time curves for the unsaturated penetration of silicone oil into glass fiber bundles with fiber volume fraction of 60% under the assistance of applied vacuum and compressed air, respectively.

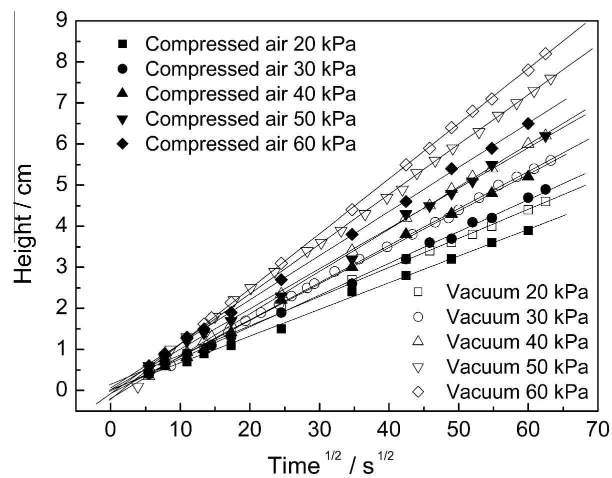

Fig. 3. Height-square root of time plots of silicone oil penetrated into glass fiber bundles with fiber volume fraction of 60%, under the assistance of vacuum and compressed air, respectively.

where P_{app} represents the external applied pressure, marked as P_{app}^{va} for the external vacuum pressure and P_{app}^{co} for the compressed air pressure hereinafter. Then Eq. (4) can be integrated and rearranged as:

$$\frac{h^2}{t} = \frac{2K}{\eta(1-V_f)}(P_{\mathrm{app}} + P_c). \tag{5}$$

By defining $\psi^2 = h^2/t$ to illustrate the relative velocity of penetration flow, a linear relationship between ψ^2 and P_{app} is presented:

$$\psi^2 = \frac{2K}{\eta(1-V_f)}P_{\mathrm{app}} + \frac{2KP_c}{\eta(1-V_f)}. \tag{6}$$

Fig. 3 gives plots of impregnated fluid heights *versus* the square root of time. The graphs illustrated quite good linear relationships which indicate that Darcy's law produces a good representation of the experimental data. By plotting ψ^2 as a function of P_{app}, a straight line should fit the data with:

$$\text{slope} = a = \frac{2K}{\eta(1-V_f)}, \tag{7}$$

$$\text{intercept} = b = \frac{2KP_c}{\eta(1-V_f)}. \tag{8}$$

Hence, unsaturated permeability of fiber assembly K and the dynamic capillary pressure P_c^d can be calculated by these relations:

$$K = \frac{a\eta(1-V_f)}{2}, \tag{9}$$

$$P_c^d = \frac{b}{a}. \tag{10}$$

3. Results and discussion

3.1. Dynamic capillary pressures measured from infiltration experiments

In order to analyze the capillary effects arising from the interface action between fiber preform and the fluid, external pressures applied to the dynamic infiltration experiments were sufficiently low. For the sets of vacuum driving experiments, we plotted measured penetration flow velocities ψ^2 *versus* external pressures, P_{app}^{va}, in Fig. 4. Eq. (6) is well verified by the data points of Fig. 4 and allows us to determine the dynamic capillary pressure, P_c^d, by extrapolating the plots to zero external pressure. In the case of compressed air driving experiments, the plot of ψ^2-P_{app}^{co} also fitted a straight line in Fig. 5. Hence, the dynamic capillary pressures, averaged from the whole penetration process, can be calculated according to Eq. (10). Data obtained from experiments are summarized in Table 2 for silicone oil penetrated into unidirectional glass fiber bundles with different fiber volume fractions, 50%, 60%, 70%, and driven by vacuum and compressed air, respectively. Besides, quasi-static capillary pressures, P_c^s, are also listed in Table 2 which

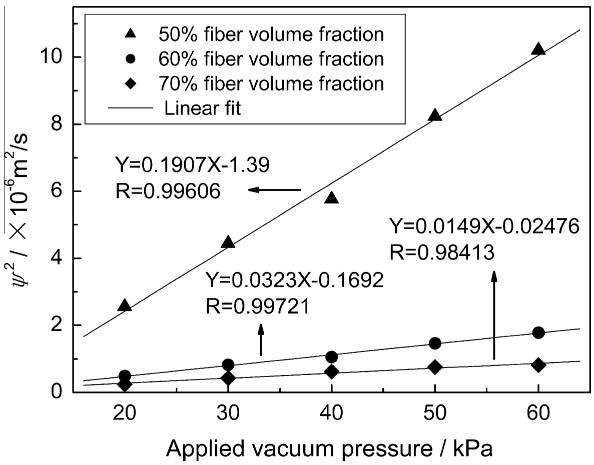

Fig. 4. Plots of ψ^2 as a function of the external vacuum pressures according to Eq. (6), for experiments of silicone oil permeation into the unidirectional fiber bundles with different fiber volume fractions.

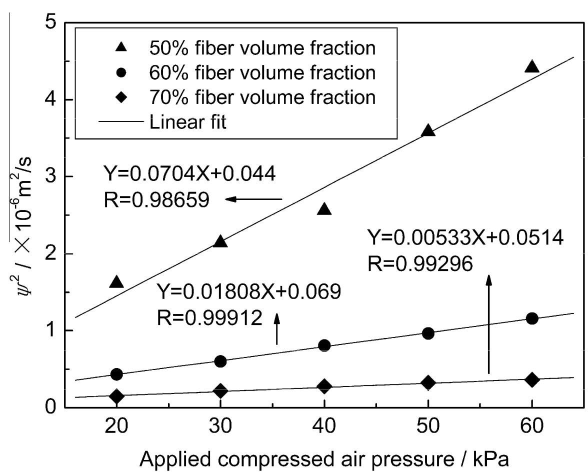

Fig. 5. Plots of ψ^2 as a function of the external compressed air pressures according to Eq. (6), for experiments of silicone oil permeation into the unidirectional fiber bundles with different fiber volume fractions.

Table 2
Dynamic capillary pressures P_c^d extrapolated from silicone oil penetration experiments in unidirectional glass fiber bundles driven by external pressures according to Eq. (10); and the quasi-static capillary pressures P_c^s calculated from tested advancing contact angles between glass fiber filaments and silicone oil according to Eq. (15).

Fiber volume fraction/%	50	60	70
P_c^d extrapolated from vacuum driving penetrations/kPa	−7.3	−5.2	−1.7
P_c^d extrapolated from compressed air driving penetrations/kPa	0.6	3.8	9.6
P_c^s calculated from advancing contact angles/kPa	6.8	10.3	16

are calculated from advancing contact angle between glass fiber filaments and silicone oil applied to idealized uniform capillary tubes according to Young–Laplace equation. Details are explicated in Section 3.3.1.

For compressed air driving penetration, the extrapolated capillary pressure (Table 2) are all positive values, illustrating promotive synergistic effect of capillary force. Moreover, variation of the capillary pressure indicated a stronger effect when fiber volume fractions increased, which is consistent with the tendency of the quasi-static pressures. The values of both P_c^d and P_c^s in Table 2 are all about or lower than 10 kPa, in same order as reported by Amico and Lekakou [23] in single fiber bundle.

However, for vacuum driving penetration, the extrapolated dynamic capillary pressures are all negative (Table 2), obviously distinct from those obtained from compressed air driving experiments. The minus P_c^d are similar to the capillary pressure, −13.9 kPa reported by Manson and coworkers [14], where non-crimp fabrics were infiltrated with an epoxy resin. If values of these dynamic capillary pressures are reliable, if can be inferred that meniscus shape of the flow front in vacuum driving penetration is inverted with respect to the flow direction, illustrating a unique drag effect of capillary action. This is very important not only for measurement of unsaturated permeability, but also for the voids formation and micro-flow simulation in vacuum-based liquid composite moulding.

Consequently, fiber holders with much bigger diameters, 8 mm of inner diameter were used to conduct silicone oil infiltration to investigate the size effect by contrast with those carried out with 3.8 mm holder, where 308 and 67 bundles were used respectively, to keep the fiber volume fraction controlled at 60%. The resulted data in Fig. 6 exhibits very small difference between these two sets. Dynamic capillary pressure for the 8 mm holder is evaluated to be −6.8 kPa by linear fitting, for the 3.8 mm holder as −5.2 kPa, indicating a slight influence of the holder size.

It should be explicitly mentioned that, for the vacuum driving penetration experiments, the extrapolated capillary pressures increase, i.e. the absolute values of the capillary pressure decrease with increasing fiber fractions, which cannot be explicated by thermodynamic theory. This variation is exactly opposite to that in compressed air driving experiments where the capillary pressure acts stronger stimulative effect on the penetration with increasing fiber fractions. Especially, for the 70% fiber fraction experiment of vacuum driving penetration, the data of −1.7 kPa (Table 2) indicates almost negligible influence of capillary pressure. This phenomenon gives us a hint on the consideration of critical factors which determines the drag or promotive effect of capillary force acting on the velocity of penetration flow in liquid composite moulding under the assistance of vacuum.

3.2. Synergetic effects of dynamic capillary pressures in vacuum driving penetrations

3.2.1. Correlation between Ca and dynamic capillary pressures

Hoffman found that the wetting angle is dependent on the forced velocity of the gas–liquid interface when a wetting liquid displaces a nonwetting fluid in a capillary tube [17]. And capillary

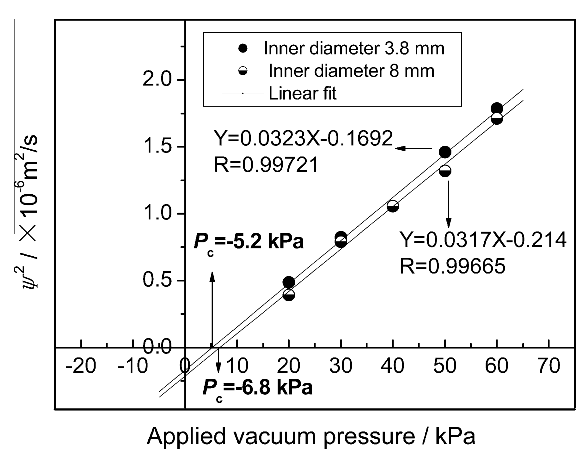

Fig. 6. Plots of ψ^2 *versus* the external vacuum pressures, for silicone oil permeation experiments conducted by preform holder with 3.8 mm and 8 mm inner diameters, where 67 and 308 bundles were used, respectively for the 60% fiber volume fraction.

number, *Ca*, is proven to be very useful to analyze the advancing liquid–air interface in which viscous and interfacial forces are the dominant factors controlling the system. It is a dimensionless velocity, defined as ratio of viscous forces to interfacial forces at the gas–liquid interface $Ca = \eta \cdot u/\gamma$, where η and γ are viscosity and surface tension of liquid, and u is the velocity of the interface. It can be seen from Fig. 2 that the fluid velocity decreased with increasing permeation time, which resulted in relatively smaller *Ca*. During a given experiment in this study, such as silicone oil permeated into unidirectional fiber bundles with 60% fiber volume fraction, the flow velocity typically varies from beginning of 1.0×10^{-4}m/s to 6.7×10^{-6}m/s at quasi-steady state where $Ca_{max} = 11.4 \times 10^{-4}$ (Table 3), $Ca_{min} = 7.5 \times 10^{-5}$ (not shown). Hence, we choose time range of 0–100 s and 400–600 s to analyze the fast and middle transient velocities of the impregnation. Plots of transient ψ^2 *versus* applied vacuum, P^{va}_{app}, are shown in Fig. 7. By extrapolating ψ^2-P^{va}_{app} plots to zero external pressure, capillary pressures can be calculated as −8.0 kPa and −3.3 kPa, for the 0–100 s and 400–600 s time ranges, respectively. These values both are different from the mean capillary pressure, −5.2 kPa averaged over the whole penetration process (Table 2).

In order to have a further insight on dynamic effect of capillary action on vacuum driving impregnation, correlations between capillary pressures and the corresponding capillary numbers should be considered in details. We evaluated dynamic capillary pressures by transient velocities, i.e. ψ^2 over the time range of 0–100 s and 400–600 s respectively. The data are displayed in Table 3 together with the corresponding capillary numbers. From Table 3, it can be seen that all the transient capillary pressures differ from those mean values (Table 2) resulted from a whole infiltration flow. Moreover, for the same experiment, greater values of *Ca* always correlated to larger size of capillary pressure. Therefore, a definite conclusion can be drawn that dynamic capillary pressures vary depending on the velocity of penetration, totally different from the thermodynamic capillary pressure estimated by Young equation. As infiltration going on, the interfacial effect gradually becomes stronger in competition with the viscous effect, and the dynamic capillary pressure closely related to the capillary number.

From Table 3, we can also find that the transient dynamic capillary pressures exhibit all minus sign, except one, the 0.8 kPa for penetration in 70% fiber faction bundles within time range of 400–600 s. Although data of this set scattered relatively wider than penetrations in 60% and 50% fiber content bundles, plots of transient ψ^2 *versus* P^{va}_{app} still fitted in straight line to give a reliable dynamic capillary pressure. For the only positive capillary pressure of 0.8 kPa, it corresponds with the minimum *Ca* in Table 3, less than 1.7×10^{-4}, while most capillary pressures present to be minus for *Ca* larger than this critical value. Similar features have already been reported by Calvo et al. [19] for diphasic flow in glass capillary tubes, where dynamic capillary pressure becomes negative at the same magnitude of capillary number. Also, Weitz et al. [18] indicated that dynamic capillary pressure changes sign at different value of capillary number for different porous medium. Therefore, we can conclude that negative capillary pressures definitely present the dynamic synergistic effect of interfacial force on velocity of vacuum driving penetration in unidirectional fiber bundles, where viscous and interfacial forces are the dominant flow regime.

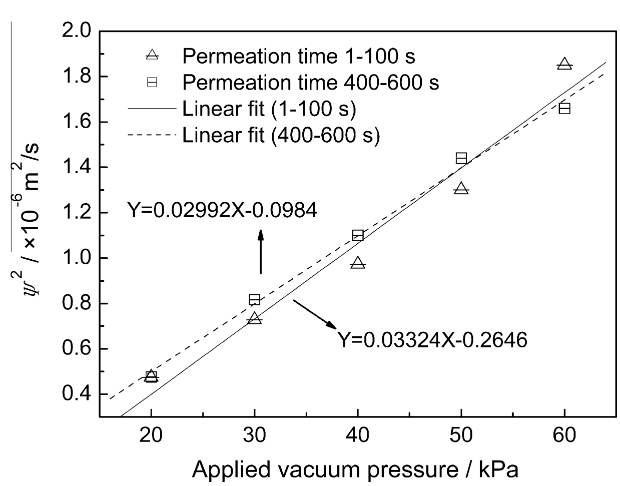

Fig. 7. Plots of transient ψ^2 at a permeation time range (1–100 s or 400–600 s) *versus* the external applied vacuum, for experiments conducted by silicone oil in unidirectional fiber bundles with 60% volume fraction.

Table 3
Dynamic capillary pressures extrapolated from transient velocities at the beginning and the medium of a penetration run, as well as the corresponding capillary number, the experiments were conducted by vacuum driving permeation of silicone oil into unidirectional fiber bundles.

	External pressure/kPa	Penetration time range of 0–100 s		Penetration time range of 400–600 s	
		$Ca/\times 10^{-4}$	P^d_c/kPa	$Ca/\times 10^{-4}$	P^d_c/kPa
Fiber volume fraction of 50%	20	13.0	−7.9	3.7	−4.2
	30	19.2		5.0	
	40	20.4		5.9	
	50	25.3		6.3	
	60	27.8		7.8	
Fiber volume fraction of 60%	20	5.4	−8.0	1.7	−3.3
	30	7.5		2.3	
	40	7.7		2.6	
	50	11.4		2.7	
	60	11.2		3.4	
Fiber volume fraction of 70%	20	4.8	−2.6	1.1	0.8
	30	5.8		1.8	
	40	6.7		2.1	
	50	9.1		2.1	
	60	8.0		2.5	

3.2.2. Curvature of the penetration flow front corresponding to the capillary effect

In order to illustrate the specific effect of capillary force in the impregnation, meniscus of flow front was theoretically calculated according to Laplace equation applied to uniform capillary tubes equivalent to the experimental data. The pressure difference across liquid–air interface at the flow front is as follows:

$$\Delta P = P^d_c = \frac{2\gamma}{R}. \tag{11}$$

Hence, R, the radius of the sphere interface at the flow front can be determined by rearranging Eq. (11),

$$R = \frac{2\gamma}{P^d_c}. \tag{12}$$

Assuming that porous unidirectional fiber bundle is a collection of idealized uniform capillary tubes, the equivalent radius r_c can be calculated as a function of fiber volume fraction and fiber radius,

$$r_c = r_f \frac{1 - V_f}{V_f} \tag{13}$$

Based on the experimental extrapolated dynamic capillary pressures in Table 2, protruding flow fronts for the vacuum driving penetrations in unidirectional fiber bundles are illustrated schematically in Fig. 8. It displays that curvature of the convex meniscus decreases with increasing fiber content (decreasing equivalent radius r_c) in vacuum driving infiltration. This tendency is very opposite to those capillary effects in compressed air driving impregnation, whose concave meniscuses increase when fiber content increases, shown in Fig. 9.

In order to validate the theoretically inferred meniscus flow front in fiber bundles, capillary flow in glass tube was visually tested by using OCA20 Dataphysics Instrument, with the assistance of vacuum and compressed air, respectively of about 1 kPa.

Glass tubes with three different inner diameters, 2 mm, 1 mm, and 0.5 mm were employed. Fig. 10 displays convex meniscus flow fronts for the vacuum driving flow, which agree well with the calculated penetration flow fronts in unidirectional fiber bundles (Fig. 8). Additionally, apparent contact angles were measured to be 166°, 128° and 102° corresponding to the radius of glass tube, 2 mm, 1 mm, and 0.5 mm. This phenomenon verifies the relationship between extrapolated dynamic capillary pressures with the fiber content in fiber bundles penetration experiments. For the compressed air driving capillary flow in glass tube, pictures of the meniscus flow front are exhibited in Fig. 11. The variation trend of the flow front with the diameter of capillary tube is consistent with the penetration results in unidirectional fiber bundles, which

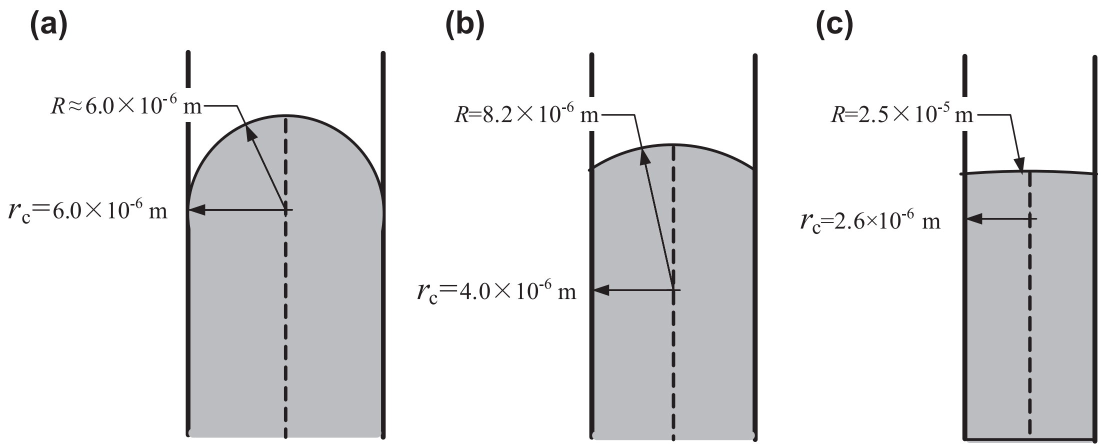

Fig. 8. Schematic of the convex meniscus flow front of penetration driven by external vacuum, which is illustrated in idealized uniform capillary tubes with the radius equivalent to unidirectional fiber assemblies with fiber volume fractions of: (a) 50%, (b) 60%, (c) 70%, respectively. The values were calculated by P_c^d, Eqs. (12) and (13) for silicone oil experiments.

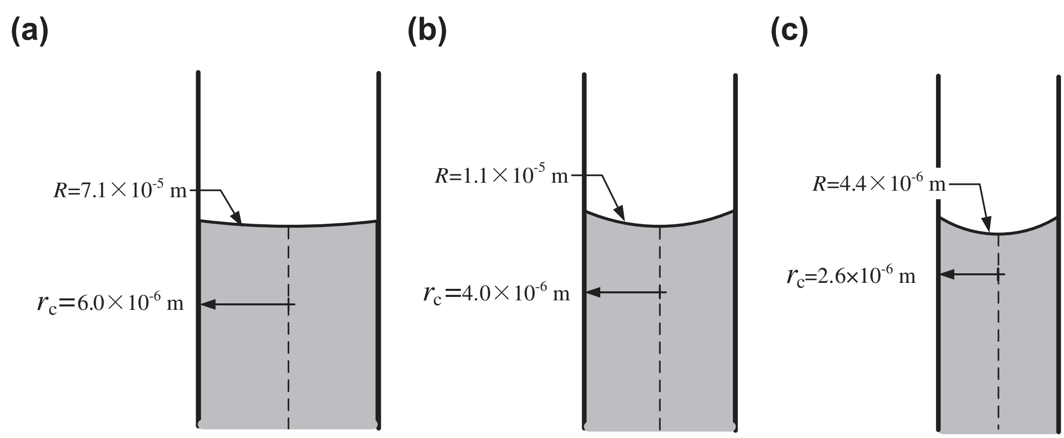

Fig. 9. Schematic of the concave meniscus penetration flow front of penetration driven by external compressed air illustrating in idealized uniform capillary tubes equivalent to unidirectional fiber assemblies with fiber volume fractions of: (a) 50%, (b) 60%, (c) 70%, respectively. The values were calculated by P_c^d, Eqs. (12) and (13) for silicone oil experiments.

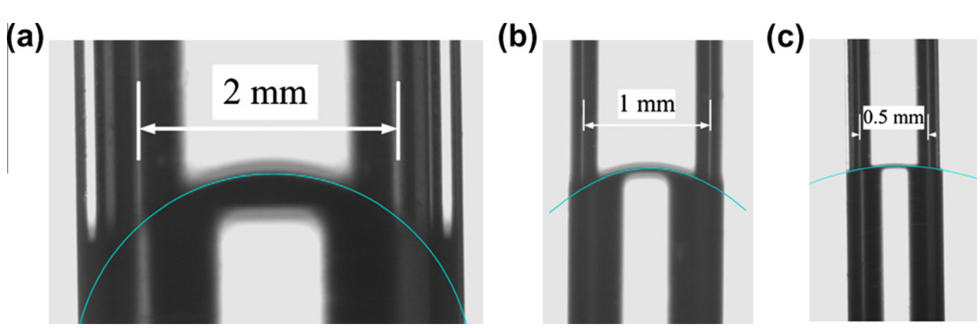

Fig. 10. Experimental pictures of convex meniscus penetration flow fronts of silicone oil driven by about 1 kPa external vacuum in capillary glass tube with inner diameters of: (a) 2 mm, (b) 1 mm, and (c) 0.5 mm and the corresponding apparent contact angles were measured to be 166°, 128° and 102°, respectively.

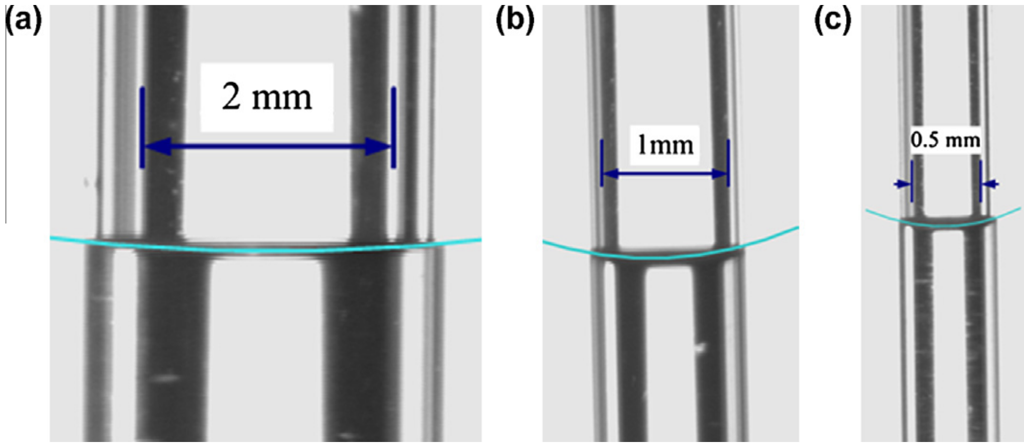

Fig. 11. Pictures of concave meniscus penetration flow fronts driven by about 1 kPa external air pressure in capillary glass tube with inner diameter of: (a) 2 mm, (b) 1 mm, and (c) 0.5 mm, respectively, and the corresponding apparent contact angles were measured to be about 85°, 78° and 75°.

are schematically illustrated in Fig. 9. Besides, it is found that meniscus flow front is closely related with the interface velocity.

In conclusion, the flow front shapes tested in glass tube verified the validity of the synergetic action of dynamic capillary pressure on the penetration flow in fiber bundles, especially for the drag effect in vacuum driving cases, which is attributed to the variation of chemical composition at the liquid–gas interface. In the vacuum driving system, gasified silicone oil will exist to change the liquid–gas interface, while in the compressed air driving cases the liquid–air interface will be exactly the same as normal.

3.2.3. Influence of fluid type on the dynamic capillary pressure of vacuum driving penetration in fiber bundles

As for the drag effect of capillary pressure found in penetration of silicone oil, one would wonder whether it is peculiar to silicone oil or universal to other typical fluids used in processing measurements of RTM, such as soybean oil, corn syrup, and epoxy resin. Consequently, soybean oil, epoxy resin and glycerol were also employed to investigating the capillary effect on impregnating into unidirectional fiber bundles with the volume fraction of 60%. The ψ^2-P^{va}_{app} diagrams of these three fluids were plotted in Fig. 12 together with silicone oil for contrast. And the extrapolated capillary pressures were listed in Table 4, as well as the *Ca* and the infiltration velocity at liquid height of about 2.5 cm in fiber bundles. It can be found that the capillary pressure for soybean oil was calculated to be −3.4 kPa with negative signs, similar with silicone oil. However, capillary pressures for glycerol and epoxy resin came out to be 6.2 kPa and 9.6 kPa, suggesting positive synergistic effect. As proved by Section 3.2.1, these positive capillary pressures were due to the capillary number, which fell behind a sort of critical value determined by the system and the flow velocity.

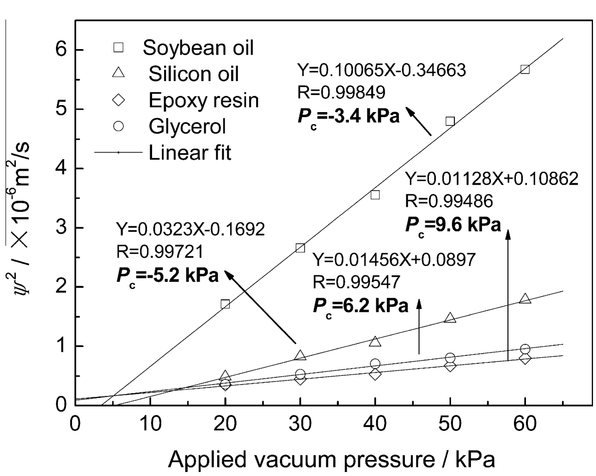

Fig. 12. Plots of ψ^2 as a function of the external applied vacuum pressures according to Eq. (6), for different fluids permeating into unidirectional fiber bundles with the fiber volume fraction of 60%.

3.3. Effect of capillary pressure on the estimation of unsaturated permeability of inner fiber tows

3.3.1. Theoretically-estimated capillary pressures according to thermodynamic principles

Furthermore, in order to analyze the influence of capillary pressure on the unsaturated permeability of fiber bundle, quasi-static capillary pressure has been estimated based on thermodynamic principles in equivalent idealized uniform capillary tubes. Advancing contact angle between single fiber and liquid was measured by Wihelmy plate method to calculate the quasi-static capillary pressure.

In the experiments, five fiber filaments were suspended in parallel onto a balance of tensionmeter DCAT21, and the liquid was then raised to contact the filaments at a speed of 30 μm/s to detect the wetting force, then advancing contact angle could be calculated by [24]:

$$\cos\theta = \frac{F}{\gamma P} \tag{14}$$

where F is the wetting force measured by the balance, P is filament perimeter which was measured by the metallographic picture of the glass fiber bundle cross-section as shown in Fig. 13, and γ and θ are surface tension of testing fluid and advancing contact angle, respectively.

By combination with Eq. (13), quasi-static capillary pressure P_c^s may be theoretically estimated using the Young–Laplace equation [25], as follows:

$$P_c^s = \frac{2FV_f}{r_f P(1-V_f)} \tag{15}$$

Since tested advancing contact angle of silicone oil to glass fiber was 16.7°, the values of quasi-static capillary pressures P_c^s in equivalent fiber bundles are calculated and listed in Table 2. It is found that these theoretically estimated P_c^s s are all about the same magnitude, but larger than the dynamic experimental extrapolated P_c^d ones. Moreover, theoretically calculated quasi-static capillary pres-

Table 4
Extrapolated dynamic capillary pressures for different fluids permeated into fiber bundles (60% volume fraction) driven by external vacuum pressure of 40 kPa, the corresponding velocity with infiltration height of 2.5 cm as well as the capillary numbers.

Fluids	Silicone oil	Soybean oil	Epoxy resin	Glycerol
P_c^d extrapolated from vacuum driving penetration/kPa	−5.2	−3.4	9.6	6.2
Velocities at 2.5 cm infiltration height in fiber bundles/$\times 10^{-5}$m/s	2.0	7.2	1.0	1.3
Capillary numbers corresponding to the velocity above/$\times 10^{-4}$	2.3	1.7	1.5	1.0

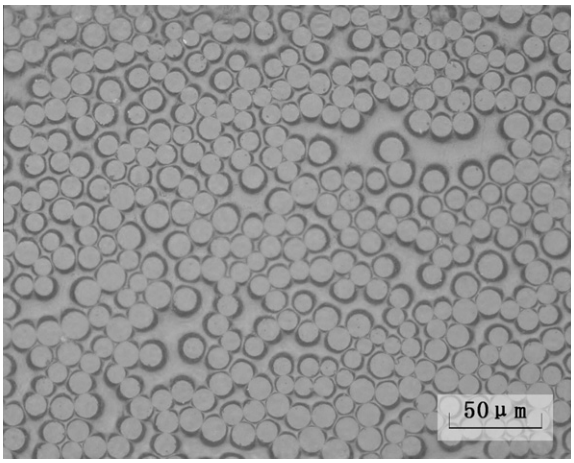

Fig. 13. Metallographic picture of the cross-section in glass fiber bundles.

sure increases with increasing fiber fractions, which is in agreement with the extrapolated result from compressed air driving penetration but opposite to that from vacuum driving infiltration.

3.3.2. Effect of capillary pressure on the estimation of unsaturated permeabilities

Permeability expresses how easy it is for a liquid to penetrate a porous medium, and it is a critical parameter for analyzing the resin flow in RTM injection process. In the unsaturated penetration cases, capillary pressure, P_c, presents a significant driving force for resin impregnation and, therefore, should be taken into account to optimize the RTM process. In order to investigate the influence of capillary pressure on the value accuracy of axial unsaturated permeability, experimental permeabilities of glass fiber bundles were analyzed in this study. Firstly, the permeabilities determined solely from external pressure driving penetrations were calculated according to Eq. (5) by neglecting capillary pressure. Table 5 shows the results of unidirectional glass fiber bundles with 60% fiber volume fraction. From the data we can find that the average permeability resulted from compressed air driving experiment turns out to be $K = 0.96 \times 10^{-12}$ m^2, while the permeability from vacuum driving infiltration exhibits a larger value as $K = 1.31 \times 10^{-12}$ m^2. This might be due to the fiber rearrangement happened in vacuum assisted experiment, where the convex flow fronts expand the distance between individual fibers inside the tows.

For comparison, corrected permeabilities were also analyzed by taking the capillary pressures into consideration, as given in Table 5. It can be found that, for the compressed air driving penetrations, the corrected permeabilities are all smaller than those obtained by neglecting capillary force. On the contrary, for the vacuum driving penetrations, the corrected permeabilities are all bigger than those calculated by neglecting capillary action. These apparent discrepancies demonstrate that longitudinal micro-flow driven by capillary pressure in the unidirectional fiber bundle is a critical term in determining the axial unsaturated permeability.

As an important material parameter, permeability is theoretically only dependent on the geometry of fiber bed, which was consistent with the test results of permeabilities by different fluids. A great deal of effort has been devoted to establish mathematical and theoretical model to predict it. For regularly aligned fiber assembly, axial permeability along the fibers can be expressed as Eq. (16) according to the empirical Kozeny–Carman Equation [26,27]:

$$K = \frac{r_f^2}{4k_0}\frac{(1-V_f)^3}{V_f^2} \tag{16}$$

where k_0 is Kozeny constant, a factor represents shape and the tortuosity of the flow path, whose theoretical value is supposed to be two for axial infiltration.

Average Kozeny constant of unidirectional fiber bundle was analyzed in this paper, based on capillary pressure-corrected permeabilities from the longitudinal penetration experiments driven by compressed air and vacuum, respectively. Fig. 14 shows plots of the corrected permeabilities as a function of $(1-V_f)^3/V_f^2$ for the penetration experiments conducted under 40 kPa external pressure by Eq. (16). As can be seen, the data for the different experiments fitted a good straight line in Fig. 14, where the Kozeny constant of compressed air driving penetration was calculated as $k_0 = 1.1$, which was very close to the previous study by Batch [20] (1.06 resulted from capillary impregnation experiment). On the other hand, for the vacuum driving penetration, the Kozeny

Table 5
Calculated axial unsaturated permeability of unidirectional glass fiber bundles of 60% volume fraction, neglecting or taking consideration of the dynamic capillary pressures in Table 2.

External applied pressures/kPa		20 kPa	30 kPa	40 kPa	50 kPa	60 kPa	Average permeability
Permeabilities calculated from compressed air driving penetrations/$\times 10^{-12}$ m^2	Neglecting P_c	1.03	0.95	0.96	0.92	0.92	0.96
	Taking extrapolated P_c^d into consideration	0.87	0.85	0.88	0.85	0.86	0.86
	Taking theoretically estimated P_c^s into consideration	0.68	0.71	0.77	0.76	0.78	0.74
Permeabilities calculated from vacuum driving penetrations/ $\times 10^{-12}$ m^2	Neglecting P_c	1.16	1.31	1.26	1.39	1.42	1.31
	Taking extrapolated P_c^d into consideration	1.57	1.58	1.44	1.55	1.55	1.54

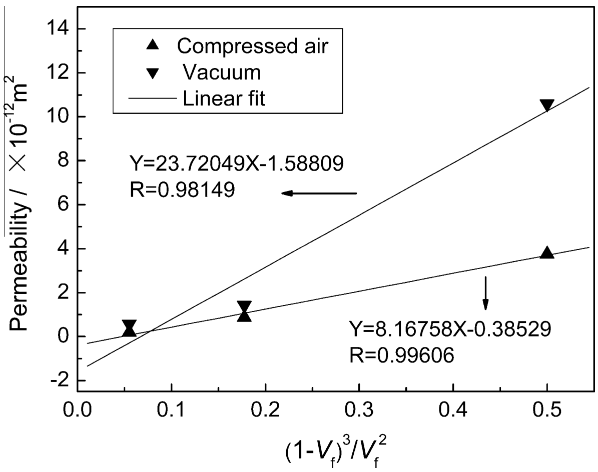

Fig. 14. Plots of axial unsaturated permeability of unidirectional fiber bundles corrected by extrapolated dynamic capillary pressure P_c^d *versus* the $(1-V_f)^3/V_f^2$ according to Eq. (16), for the penetration experiments conducted by silicone oil under 40 kPa external pressures.

constant was calculated to be 0.37, very similar to the value of 0.35 reported by Lam for the silicone oil penetrated in unidirectional fiber beds [28], which was conducted under applied mechanical pressure. The result displayed a much lower k_0 in comparison with the case for compressed air driving experiment, which further demonstrated the influence of type of applied external pressure on the geometry of fiber bundle.

4. Conclusions

A simple method was developed to investigate synergetic effect of capillary action on the velocity of axial infiltration in unidirectional fiber bundles with assistance of external pressures either vacuum or compressed air. Dynamic capillary pressures can be calculated by extrapolating ψ^2–P_{app} plot to zero applied pressure.

It is found that the extrapolated dynamic capillary pressures are all negative in vacuum driving permeation of silicone oil into fiber bundles, indicating unique drag effects, which is inconsistent with the results in compressed air driving experiments. Analysis of the shape of the infiltration flow front demonstrates that the negative values of capillary pressure definitely presents drag effect of interfacial force on the dynamic of vacuum driving penetration into unidirectional fiber bundles. The mechanism behind this effect is currently unknown and further work is required to elucidate it fully. Moreover, the synergetic effects, either drag or promotive force of capillary pressure are proved to have close relationship with the capillary number of the penetration. This would be helpful to the analysis of mould filling and defects formation in vacuum assisted resin transfer moulding process.

Meanwhile, both theoretically calculated quasi-static capillary pressures according to Young–Laplace equation and extrapolated dynamic capillary pressures from infiltration experiments are of the same magnitude. Variation tendency of quasi-static capillary pressure with fiber volume fraction agrees well with the extrapolated dynamic results from compressed air driving penetration but opposite to those from vacuum driving infiltration.

Besides, the unsaturated permeability can be precisely corrected by the dynamic capillary pressure extrapolated from infiltration experiments. And Kozeny constants were determined as 1.1 for permeability of unidirectional fiber bundles from compressed air driving infiltration, and 0.37 for the vacuum driving cases, suggesting that type of the applied external pressure could impact on geometry of the fiber assemblies. Moreover, permeabilities from vacuum driving infiltrations were found to be bigger than from compressed air tests.

Acknowledgements

This work was supported by funding from the National Natural Science Fund Program of China (50803002) and Aviation Science Fund (2008ZE51072).

Reference

[1] Kang MK. A dual-scale analysis of macroscopic resin flow in vacuum assisted resin transfer molding. Polym Compos 2004;25(5):510–20.
[2] Gutowski TG, Cai Z, Bauer S, Boucher D. Consolidation experiment for laminate composites. J Compos Mater 1987;21:650–69.
[3] Gebart BR. Permeablity of unidirectional reinforcement for RTM. J Compos Mater 1992;26(8):1100–33.
[4] Vd Westhuizen J, Du Plessis P. Quantification of unidirectional fiber bed permeability. J Compos Mater 1994;28(7):619–37.
[5] Pillai KM, Advani SG. Wicking across a fiber-bank. J Colloid Interface Sci 1996;183:100–10.
[6] Zhou F, Kuentzer N, Simacek P, Advani SG, Walsh S. Analytic characterization of the permeability of dual-scale fibrous porous media. Compos Sci Technol 2006;66(15):2795–803.
[7] Zhou F, Alms J, Advani SG. A closed form solution for flow in dual scale fibrous porous media under constant injection pressure conditions. Compos Sci Technol 2008;68(3–4):699–708.
[8] Acheson JA, Simacek P, Advani SG. The implications of fiber compaction and saturation on fully coupled VARTM simulation. Compos Part A – Appl Sci Manuf 2004;35:159–69.
[9] Simacek P, Advani SG. A numerical model to predict fiber tow saturation during liquid composite molding. Compos Sci Technol 2003;63:1725–36.
[10] Luo Y, Verpoest I, Hoes K, Vanheule M, Sol H, Cardon A. Permeability measurement of textile reinforcements with several test fluids. Compos Part A – Appl Sci Manuf 2001;32:1497–504.
[11] Kuentzer N, Simacek P, Advani SG, Walsh S. Correlation of void distribution to VARTM manufacturing techniques. Compos Part A – Appl Sci Manuf 2007;38:802–13.
[12] Patel N, Rohatgi V, Lee LJ. Micro scale flow behavior and void formation mechanism during impregnation through a unidirectional stitched fiberglass mat. Polym Eng Sci 1995;35(10):837–51.
[13] Ahn KJ, Seferis JC. Simultaneous measurements of permeability and capillary pressure of thermosetting matrices in woven fabric reinforcements. Polym Compos 1991;12(3):146–52.
[14] Verrey J, Michaud V, Manson JAE. Dynamic capillary effects in liquid composite moulding with non-crimp fabrics. Compos Part A – Appl Sci Manuf 2006;37:92–102.
[15] Amico S, Lekakou C. An experimental study of the permeability and capillary pressure in resin transfer moulding. Compos Sci Technol 2001;61:1945–59.
[16] Lawrence JM, Neacsu V, Advani SG. Modeling the impact of capillary pressure and air entrapment on fiber tow saturation during resin infusion in LCM. Compos Part A – Appl Sci Manuf 2009;40:1053–64.
[17] Hoffman RL. A study of the advancing interface 1. Interface shape in liquid–gas systems. J Colloid Interface Sci 1975;50:228–41.
[18] Weitz DA, Stokes JP, Ball RC, Kushnick AP. Dynamic capillary pressure in porous media: origin of the viscous-fingering length scale. Phys Rev Lett 1987;59:2967–70.
[19] Calvo A, Paterson I, Chertcoff R, Rosen M, Hulin JP. Dynamic capillary pressure variations in diphasic flows through glass capillaries. J Colloid Interface Sci 1991;141:384–94.
[20] Batch GL, Chen YT, Macosko CW. Capillary impregnation of aligned fibrous beds: experiments and model. J Reinf Plast Compos 1996;15:1027–51.
[21] Perrin CL, Tardy PMJ, Sorbie KS, Crawshaw JC. Experimental and modeling study of Newtonian and non-Newtonian fluid flow in pore network micromodels. J Colloid Interface Sci 2006;295(2):542–50.
[22] Bayldon JM, Daniel IM. Flow modeling of the VARTM process including progressive saturation effects. Compos Part A – Appl Sci Manuf 2009;40(8):1044–52.
[23] Amico SC, Lekakou C. Axial impregnation of a fiber bundle. Part 1: capillary experiments. Polym Compos 2002;23(2):249–63.
[24] Pezron I, Bourgain G, Queret D. Imbibition of a fabric. J Colloid Interface Sci 1995;173:319–27.
[25] Kornev KG, Neimark AV. Spontaneous penetration of liquid into capillaries and porous membranes revisited. J Colloid Interface Sci 2001;235:101–13.
[26] Xu P, Yu B. Developing a new form of permeability and Kozeny–Carman constant for homogeneous porous media by means of fractal geometry. Adv Water Resour 2008;31(1):74–81.
[27] Cai Z. Estimation of the permeability of fibrous preforms for resin transfer moulding processes. Compos Manuf 1992;3(4):251–7.
[28] Lam RC, Kardos JL. The permeability and compressibility of aligned and cross-plied carbon fiber beds during processing of composites. Polym Eng Sci 1991;31(14):1064–70.